

Stoichiometric analysis of the energetics and metabolic impact of photorespiration in C3 plants

Benazir Huma^a, Sudip Kundu^{a*}, Mark G. Poolman^b, Nicholas J. Kruger^c and David A. Fell^b

a Department of Biophysics, Molecular Biology and Bioinformatics,
University of Calcutta,
92 APC Road,
Kolkata 700 009,
West Bengal,
India

b Department of Biological and Medical Sciences,
Oxford Brookes University,
Gipsy Lane,
Headington,
Oxford, OX3 0BP
UK

c Department of Plant Sciences,
University of Oxford,
South Parks Road,
Oxford, OX1 3RB
UK

*For editorial correspondence and proofs. Email: skbmbg@caluniv.ac.in; Tel: +91 94334 28324

Running title

Elementary Modes Analysis of Photorespiration

Keywords

Photorespiration; C3 plants; metabolic modelling; elementary modes analysis; nitrogen metabolism; assimilation quotient.

Summary

Analysis of the impact of photorespiration on plant metabolism is usually based on manual inspection of small network diagrams. Here we create a structural metabolic model that contains the reactions that participate in photorespiration in the plastid, peroxisome, mitochondrion and cytosol and the metabolite exchanges between them. This model was subjected to elementary flux modes analysis, a technique that enumerates all the component, minimal pathways of a network. Any feasible photorespiratory metabolism in the plant will

This article has been accepted for publication and undergone full peer review but has not been through the copyediting, typesetting, pagination and proofreading process, which may lead to differences between this version and the Version of Record. Please cite this article as doi:

10.1111/tpj.14105

This article is protected by copyright. All rights reserved.

Accepted Article

be some combination of the elementary flux modes (EFMs) that contain the Rubisco oxygenase reaction. Amongst the EFMs we obtained was the classic photorespiratory cycle, but there were also modes that involve photorespiration coupled with mitochondrial metabolism and ATP production, the glutathione-ascorbate (GSH-ASC) cycle and nitrate reduction to ammonia. The modes analysis demonstrated the underlying basis of the metabolic linkages with photorespiration that have been inferred experimentally. The set of reactions common to all the elementary modes showed good agreement with the gene products of mutants that have been reported to have a defective phenotype in photorespiratory conditions. Finally, the set of modes provided a formal demonstration that photorespiration itself does not impact on the $\text{CO}_2:\text{O}_2$ ratio (assimilation quotient, AQ), except in those modes associated with concomitant nitrate reduction.

1 Introduction

Photorespiration or the C2 cycle is one of the major carbon metabolism pathways in plants, second only to photosynthesis occurring at about 30-100% the rate of photosynthesis in C3 crop plants, depending on environmental conditions (Oliver, 2000). It is the pathway through which terrestrial plants process the carbon in 2-phosphoglycolate (2-PG) that is the product of the ribulose-1,5-bisphosphate (RuBP) oxygenase activity. This comes at the expense of energy and generation of photorespiratory CO_2 . Therefore, photorespiration has generally been regarded as a wasteful process and it has long been contested that by inhibiting the oxygenase reaction, and therefore photorespiration, crop yield could be increased (Zelitch, 1973). This is debatable given the importance of photorespiration in plant survival and productivity (Aliyev, 2012; Bloom, 2015; Hodges et al., 2016) and its interactions with multiple cellular metabolic pathways (Foyer et al., 2009; Bauwe et al., 2012; Florian et al., 2013; Hodges et al., 2016; Busch et al., 2017).

The C2 cycle starts in the chloroplast with RuBP reacting with O_2 to form a 3-phosphoglycerate (3-PGA) which can continue in the C3 cycle and a 2-PG that must be recovered to prevent accumulation of a toxic intermediate and to allow return of its carbon into the C3 cycle (Fig.1). The reactions and intracellular compartmentation of the conventional C2 cycle are shown in Fig.1.

Apart from its impact on the carbon economy of the cell, photorespiration has potential implications for plastidial and cellular ATP and NAD(P)H turnover, overall quantum demand (QD: photon demand per unit of CO_2 fixed), and the assimilation quotient (AQ: CO_2 fixed per O_2 released). To date, the calculations of these impacts have been based on various assumptions about the structure of the pathway and have been carried out by manual accounting for the coenzyme requirements, generally against a background of photosynthetic assimilation (Wingler et al., 2000; Oliver, 2000; Noctor and Foyer, 1998; Foyer et al., 2009).

There is increasingly strong experimental evidence that there is a positive coupling between photorespiration and nitrogen assimilation (Searles and Bloom, 2003; Rachmilevitch et al., 2004; Bloom, 2015; Busch et al., 2017), though conventional representations of the photorespiratory cycle do not illustrate any direct mechanism for this. Noctor and Foyer (1998) carried out calculations of the changes in energetics when photorespiration and NO_3^- assimilation to amino acids occur in parallel at rates characteristic for C3 plants, but again did not point to a specific mechanism to explain this. Entangled with this is the relationship between the value of AQ and the occurrence of photorespiration and NO_3^- assimilation. It is known from experimental measurement and calculation that increased NO_3^- assimilation in

the light lowers AQ, as would be required to generate the reductant for NH_4^+ production. However, AQ also appears to differ depending on whether photorespiration is active or suppressed, which has led some to use change in AQ to estimate rates of photorespiration (Skillman, 2008). This was contradicted by Foyer et al. (2009) who presented an analysis showing no significant impact of photorespiration on AQ. There is therefore a need to determine whether there can be some direct effect of the occurrence of photorespiration on AQ, or whether this apparent linkage is entirely indirect via the effect of photorespiration on nitrogen metabolism.

In the previous Flux Balance Analysis (FBA) of the genome-scale model (GSM) of rice (Poolman et al., 2013, 2014) we observed that there was no impact resulting from variations in the rate of photorespiration on the modelled AQ. An observed decrease in AQ resulted from a switch in the use of N-source from ammonia to nitrate (Poolman et al., 2014). However, FBA determines a set of reaction rates in a metabolic network that optimizes some chosen outcome, such as the maximum yield of a metabolic product subject to given constraints (Fell and Small, 1986; Varma and Palsson, 1993). Therefore, this observation may not be true for a steady state away from these optima. Similarly, the argument by Foyer et al. (2009) against an impact on AQ was based on an analysis of a specific scenario.

Some interesting insights into the factors affecting the rate of photorespiration have been obtained recently using kinetic modelling by Xin et al. (2015), but the issues addressed are different from this study. The authors note that further progress with this type of modelling is hindered by the current lack of some key kinetic data, especially on transport processes. A recent higher-level kinetic model proposed by Busch et al. (2017) has attempted to integrate photoassimilation, photorespiration and concomitant nitrate reduction and suggests that there are conditions where this can lead to an increase in the maximum net assimilation rate in spite of the potential negative effect of photorespiration.

For questions related to the existence of specific pathways through a network and the overall conversions being catalysed by them, stoichiometric (or structural) modelling techniques are particularly suited (Schuster and Fell, 2007). Though this does not lead to unique predictions about the state of a cell's metabolism, it does distinguish between feasible and infeasible states and can thus delimit all the possibilities open to a defined network, whilst requiring less data than kinetic approaches.

In this study, we have developed a medium scale compartmentalized model, comprising the chloroplast, the peroxisome, the mitochondrion and cytosol, extracted from our GSMs of arabidopsis (Poolman et al., 2009; Cheung et al., 2013) and rice (Poolman et al., 2013), and used this new model to investigate the potential pathways of photorespiration using elementary flux modes analysis (EFMA) (Schuster et al., 1999; Schilling et al., 1999; Schuster et al., 2000). An elementary flux mode (EFM) of a metabolic network represents a minimal, independent metabolic sub-network that can potentially achieve a steady-state. It is minimal in the sense that deleting any enzyme in the set would prevent a steady state. Reactions can be enzymic conversions or transport reactions between compartments, and each is assigned a relative flux. By definition, an EFM is not decomposable into component EFMs. This ensures that the complete set of EFMs of a reaction network is unique. Each can be thought of as a pathway from substrates to products (external metabolites) with all internal metabolites balanced and with all irreversible reactions being used only in the thermodynamically favoured direction. Each EFM also has an overall mass-balanced stoichiometric equation associated with it that describes the overall metabolic conversion it performs on the external metabolites. In the case of exceptions such as internal cycles with no

thermodynamic driving force, and hence no net flux, this equation is empty, allowing their easy identification. If ADP, ATP and Pi are regarded as external metabolites to the network, then the overall equation will indicate the net ATP production or consumption of the mode. If the overall equation consists solely of hydrolysis of ATP, then the mode represents an energy-dissipating futile cycle in the network, again allowing its identification.

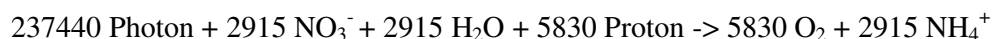
An advantage of EFMA is that whereas FBA generates a single solution that satisfies some specified optimisation criterion, the calculation of EFMs generates the total set of feasible paths through the network without the need for an imposed selection criterion. Moreover, any actual steady state of a metabolic network, and hence also any FBA solution, can always be represented as a linear combination of the of EFMs. Hence, any behaviour or conversion not represented amongst the set of modes cannot be feasible. This exhaustive analysis of the network is an advantage for small to medium-sized networks, but becomes increasingly computationally intractable as the size tends towards genome-scale metabolic networks. In particular, as any state of plant metabolism that involves simultaneous photorespiration and photoassimilation can be represented as a weighted combination of modes for the two functions, it is not necessary to consider them jointly in the first instance. Illustrations of specific scenarios can come from combinations of modes in the requisite proportions. In this study, EFMA shows that the photorespiratory cycle exists in multiple forms, a subset of which are stoichiometrically coupled to nitrate reduction.

2 Results and Discussion

2.1 Elementary Flux Modes Analysis

To generate the metabolic network model of photorespiration, we adopted a modular construction strategy by building separate models of the three organelles and using EFMA to check that each had modes that could perform the net conversions of cytosolic metabolites needed for their individual roles in photorespiration (see section 4.2, Methods S1 and Data S1). The organelle modules were then incorporated into a cellular model, along with a cytosolic module, but with no carbon-containing metabolites declared as external so that no modes involving net photoassimilation could be produced, whereas steady state photorespiration would be allowed independently of net photoassimilation (see Fig. 2 and Table S1).

Analysis of the cellular model yielded a total of 56 elementary modes involved in photorespiration, i.e. that included the Rubisco oxygenase reaction. Details of these modes are given in Appendix S1 (sections 1.1, 1.2 and 1.3) and Data S2. Note that because all the intracellular carbon metabolites are at steady state in these EFMs, the overall outcome of each mode is that the glycolate formed by the oxygenase reaction, and the CO₂ evolved in its processing, are reincorporated into the pool of metabolites. Each resulting EFM was associated with an overall metabolic conversion, allowing us to determine all possible metabolic impacts of photorespiration on the cell's economy in terms of net O₂ consumption or production (if any), photon requirement and any other net conversion. These metabolic conversions are infeasible to deduce from inspection of network diagrams. As an example, the integer stoichiometry of one of the nitrate reducing modes is:



per 15264 Rubisco oxygenase reactions (Data S2). It is intractable to manually compute modes with such integer stoichiometries.

Conventional representation of the C2 cycle as a catabolic route from 2-PG to 3-PGA that operates as an alternative to the anabolic C3 cycle tends to conceal an issue concerning their stable co-existence: for every two RuBP molecules that undergo the Rubisco oxygenase reaction, only three 3-PGA molecules are recovered (two immediately and one via the C2 cycle), so one carbon atom has been lost from the pool of Calvin cycle intermediates to the detriment of the carboxylation taking place in parallel in photoassimilation (Hodges et al., 2016). Hence the net rate of photosynthesis during photorespiration is the total rate of carboxylation minus that needed to ensure carbon maintenance in the Calvin cycle metabolites. Note that this does not imply that the specific carbon atom lost as CO₂ in photorespiration is necessarily physically recaptured by photosynthesis, only that it or a surrogate must be. However, it is indeed observed that more than 80% of the photorespiratory CO₂ is refixed (Delfine et al., 1999) and that refixation of photorespiratory and respiratory CO₂ enhances rates of photosynthesis (Busch et al., 2013). The chloroplast, mitochondrial and cytosolic isoforms of carbonic anhydrases may serve as potential players in refixation of photorespiratory CO₂ (Riazunnisa et al., 2006; Zabaleta et al., 2012).

2.2 Essential reactions of photorespiration

Within the set of 74 reactions active in at least one EFM, 43 reactions occur in everyone and hence are essential for photorespiration, since no mode can function if one of its reactions is blocked or removed. Of these 43, 26 are metabolic reactions, of which 16 can be regarded as primarily components of chloroplast photoassimilation and mitochondrial electron transport (Appendix S1: section 1.1), leaving 10 that can be regarded principally as essential reactions of photorespiration. These latter therefore might be expected to be linked to a defective phenotype under photorespiratory conditions if the genes for the proteins catalysing them were knocked down or out (Table 1).

There are, however, two known photorespiratory mutants that were not identified by the model. One is GGAT1 (reaction r19 in Fig. 2), which has a photorespiratory phenotype in arabidopsis and rice (Igarashi et al., 2003; Zhang et al., 2015), but which can be bypassed in the model by the combination of reactions r76 (AGAT) and r77, alanine aminotransferase, half the modes using the first route and the other half the second. The complication is that whilst the AGAT reaction is catalysed by GGAT1, and therefore this activity would also be lost in a GGAT1 knockout, SGAT itself has some AGAT activity and could potentially bypass the GGAT knockout. The work of Zhang et al. (2015), however, suggests that the activity of SGAT in the peroxisome is lower than that of GGAT1 and would be insufficient to carry the extra flux required when GGAT1 is knocked out in addition to its principal, essential reaction, so the phenotype is a result of a kinetic limitation that is not represented in EFMA. The other photorespiratory mutant not identified by the model is mitochondrial MDH (mitMDH), for which a 60% reduction in activity gives a defective phenotype. Some of the 56 modes do not use this reaction (as will be discussed further below), hence it was not counted as essential. The fact that there is an experimental phenotype suggests that the modes not involving mitMDH are unable to support wild-type rates of photorespiration and hence do not occur to a significant degree in the plant. Three of the known chloroplast transporters with a photorespiratory phenotype (Table 1) were also essential according to the model. However, the model also counted chloroplast oxaloacetate transport as essential, but the

known transport protein, AtpOMT1, does not give a photorespiratory phenotype when knocked out (Taniguchi et al., 2002). Despite this, as noted by Hodges et al. (2016), identification of photorespiratory transport proteins is difficult, so it is possible there are alternative carriers for the redox shuttle. Although the model contains the cytosolic reaction catalysed by HPR2, we have not included the cytosolic isoforms of either glyoxylate reductase (GR) or GLYK (Givan and Kleczkowski et al., 1992; Ushijima et al., 2017), which are unlikely to contribute substantially to photorespiratory metabolism since neither are able to compensate for the defective photorespiratory phenotype displayed by the chloroplast glycerate kinase and peroxisomal glycolate oxidase mutants. A more extended discussion of the relationships between these results and the experimental literature is given in Appendix S1: section 1.1.

2.3 Functional analysis of the elementary modes

Classification of the modes

There are four classes of modes on the basis of the overall reaction stoichiometries of the modes (Fig. S1), although they can also be classified on the basis of mitochondrial metabolism (Fig. S2):

1. 16 modes where the only net change is the absorption of photons, which we will term energy-dissipating, or futile cycles driven by photons (Figs. 3 (blue); 4 (pink/blue); S3, (yellow), and S4 (pink/yellow)).
2. 24 modes that absorb photons but recover some of the energy by phosphorylating ADP to give cytosolic ATP with no other change (Figs. 3 (red); 5 (pink/blue and red); S3 (red), and S5 (pink/yellow and red)).
3. 8 modes that absorb photons and also reduce NO_3^- to NH_4^+ , which is also accompanied by a net evolution of O_2 (Fig. 4 (green/blue) and S4 (green/yellow)).
4. 8 modes that absorb photons and produce ATP and NH_4^+ , along with O_2 (Fig. 5 (green/blue) and S5 (green/yellow)).

The energy-dissipating modes exhibit the largest flux through mitMDH, which operates to reduce oxaloacetate to malate, and which, when knocked down, generates a photorespiratory phenotype (Lindén et al., 2016). The oxaloacetate in turn is derived from malate by MDH in the cytosol and/or peroxisome. There is either a small flux through Complex I and cytochrome oxidase (COX), or a larger flux through Complex I and alternative oxidase (AOX). In either case, the protonmotive force formed as a result is consumed in NH_4^+ export. Hence these modes would allow photorespiration to absorb the energy from photons with no other net impact on cellular metabolism and could protect the photosystems from photoinhibition (Voss et al., 2013; Hodges et al., 2016). The modes shown in blue in Fig. 3 correspond to the classic view of the photorespiratory C2 cycle, except extended to include replacement of RuBP from glycerate, 3-PGA and CO_2 for carbon intermediate maintenance. This necessitates the same Calvin cycle fluxes in all the elementary modes from which we obtain the corresponding chloroplast ATP and NADPH requirements (Table S2).

In the ATP generating modes (figures as listed in class 2 above), the mitochondrial NADH from GDC is oxidised through the conventional electron transport chain or via AOX and the protonmotive force drives the synthesis of ATP that is exported to the cytosol. Studies of

mitochondrial respiratory mutants provide good evidence that some of the NADH is indeed oxidized via the electron transport chain (Dutilleul et al., 2003) although there is also evidence for this occurring via reduction of oxaloacetate to malate via mitochondrial MDH (mitMDH) activity (Hurry et al., 2005), as represented by the energy-dissipating EFMs discussed above. Of course, in the plant, it would be possible for both types of mode to operate in parallel to varying degrees.

16 of the ATP generating modes involve no mitMDH activity (e.g. Figs. 3 (red), 5 (pink/blue)) and 8 generate additional mitochondrial NADH via mitMDH through the import of malate, ultimately derived from the chloroplast, and export of oxaloacetate (e.g. Fig. 5 (red)). Given that mitMDH knockdown gives a photorespiratory phenotype (Lindén et al., 2016) the 16 ATP-generating modes that have zero flux in the mitMDH perhaps are unlikely to play a major role in the plant. In the other 8 modes, chloroplast ATP and NADPH are generated entirely by non-cyclic photophosphorylation, leading to excess reductant, as discussed further in the next section, whereas some of the former use both cyclic and non-cyclic photophosphorylation. If mitochondrial oxidation is via COX, then the ATP yields are 1.125 and 2.1 per Rubisco oxygenase reaction for the two groups of ATP-generating modes respectively. This falls to 0.375 and 0.764 if oxidation is via the AOX (Figs. S3 (red), S5 (yellow and red)). Though energy is recovered in the form of ATP to support cellular metabolism, hardly any more photons are required than for the energy-dissipating modes. However, the ATP yield is, even at best, less than a third of the amount that the same number of photons could have generated through cyclic photophosphorylation. Having ATP as a product allows for the possible coupling of the photorespiratory modes with the rest of metabolism, but since the ATP will just mix with the cellular pool, there will not be any particular processes that would be expected to have a preferential linkage. Of course, the EFMs of a complete cellular model would include modes that link all ATP-producing photorespiratory modes to each of these other metabolic processes - which would lead to thousands or more modes, but with the same overall photorespiratory characteristics. Since photorespiration occurs under conditions where there is high energy input and/or low energy demand owing to low CO₂ these modes may not normally have a physiological role.

The other route to conserve some of the energy driving the photorespiratory cycle comes from a coupling with nitrogen metabolism. In essence, surplus nitrogen which would end up in the amino acid storage pools in the vacuole is reduced and left available in the cytosol as NH₄⁺. All these 16 modes, and these modes alone, involve a net evolution of O₂ because more reductant has to be synthesised (Table 2), as is indeed evident from the atomic stoichiometry. These modes involve excess reductant generation because of complete reliance on the non-cyclic light reaction to drive photorespiration (Table 2), though part of that reductant can be shared with mitochondrial respiration for ATP generation in a subset of 8 modes that produce both (Figs. 5 (green/blue) and S5 (green/yellow)).

Amongst the energy-dissipating and ATP-generating modes, there are 16 where the glutathione-ascorbate (GSH-ASC) cycle operates in the peroxisome in parallel to CAT2 to reduce some of the H₂O₂ (e.g. Figs. 4 (pink/blue), S4 (pink/yellow), 5 (pink/blue) and S5 (pink/yellow)). However, there are no NO₃⁻ assimilating modes that use this cycle (see section 2.5). The mechanisms behind these various couplings of photorespiration with other metabolic processes are explored below.

Energetics of photorespiration

The chloroplast energy requirement of 5.0 ATP and 3.0 NADPH is an ATP:NADPH ratio of 1.67, compared with the 1.5 for operation of the Calvin cycle. The model uses an ATP:NADPH stoichiometry of 1.29 for non-cyclic photophosphorylation, so for the light reactions to balance the requirements of photorespiration it would be necessary for the contribution of cyclic photophosphorylation to be greater than that required by photoassimilation. This corresponds to the production scenario illustrated in Table 2 for the photorespiratory mode with the lowest QD. Note the slightly larger NADPH requirement when there is net formation of NH_4^+ , decreasing the required ATP:NADPH ratio from 1.69 to 1.64. If cyclic photophosphorylation cannot or does not increase beyond the level needed for photosynthesis, then meeting the photorespiratory chloroplast ATP requirement with non-cyclic photophosphorylation will lead to excess NADPH production over that used by photorespiration. The extreme case in the model is when the non-cyclic route is used exclusively; here, generating the 5.0 moles of ATP and 3.89 moles of NADPH, an excess of 0.89 moles over that needed. It is the requirement to re-oxidise this additional reductant without adding to the ATP demand that generates the metabolic couplings seen in the photorespiratory modes: nitrogen or N-assimilation, mitochondrial respiration with cytosolic ATP generation and peroxisomal reduction of H_2O_2 through the GSH-ASC cycle are all means of doing this, as can be seen from the ATP:NADPH ratios of the corresponding modes in Table 2. Evidently only processes that have an ATP:NADPH requirement lower than the 1.29 generated by non-cyclic photophosphorylation could be coupled to photorespiration to dissipate the excess reductant without creating an additional ATP demand, hence excluding the possibility that assimilation of additional CO_2 to carbohydrate or organic acids could be linked.

One unit of photorespiratory flux entails, as a minimum, a QD of 14.7 photons (values in Table 2 divided by two, as these are expressed per unit of CO_2 flux) and also requires a half unit of flux in the Rubisco carboxylase reaction. That half unit of flux in Rubisco could be driven by 4.5 photons to produce an additional 0.5 C atoms in additional triose phosphate in the photosynthetic Calvin cycle, which is less than a third of the light energy cost of photorespiration. (The photon requirement for the Calvin cycle can be calculated from EFMA of the chloroplast model -calculation shown in Data S2.) This demonstrates the ability of photorespiration to act as a considerable sink for light energy during light stress. Apart from the incurred cost of the half flux unit of Rubisco needed to recover the photorespiratory CO_2 loss, there is an implicit opportunity cost, in that the enzyme turnover resulting in the Rubisco oxygenase reaction might have been a unit of flux in the Rubisco carboxylase reaction itself, which would have only used 9 photons to fix one C atom into triose phosphate. The notional light budget would then be near balanced (14.7 compared with $9 + 4.5 = 13.5$ photons), but the cost is then apparent as a loss of assimilation of 1.5 C atoms.

Although a fraction of the additional light energy needed to support the photorespiratory cycle can be recovered in the form of NO_3^- assimilation or cytosolic ATP synthesis, the QD calculations show the effectiveness of photorespiration in combating light stress whilst minimising the net metabolic impact (Table 2). It is of interest that the coupling of photorespiration to the GSH-ASC cycle increases the QD of photorespiration at the same time as increasing the capacity for degradation of H_2O_2 in the peroxisome. There is no mode, though, where the requirement for the catalase reaction is completely suppressed; the modes using the GSH-ASC cycle are driven entirely by the non-cyclic light reaction, so there is no scope to generate the additional reductant needed to increase its flux without having a sink for the extra chloroplastic ATP that would be formed at the same time. Other potential

pathways for balancing the ATP:NADPH ratio in the chloroplast during photorespiration have been discussed in Appendix S1: section 1.4.

2.4 Photorespiration and the Assimilation Quotient

The results show that, except for the EFMs where NO_3^- is reduced to NH_4^+ , every other mode is neutral with respect to its net impact on CO_2 and O_2 (Table 2). As discussed above, the maintenance of the steady state of the Calvin cycle requires that the CO_2 lost as a result of photorespiration is replaced. However, as the analysis places no constraint on O_2 production and consumption, the finding of no impact shows that the O_2 consumed by photorespiration and any associated mitochondrial respiration is exactly balanced by O_2 production in the light reactions that drive the photorespiratory cycle plus the O_2 evolution from CAT2. Since all feasible steady states of metabolism can be expressed as a combination of EFMs, the finding that EFMs of photorespiration have no net impact on CO_2 and O_2 constitutes a general proof that photorespiration cannot impact on AQ unless linked to NO_3^- assimilation or an alternative sink for reductant of equivalent capacity.

The coupling mechanism in the nitrate-assimilating modes is the excess reductant generated by non-cyclic photophosphorylation as a by-product of making sufficient chloroplast ATP to drive the photorespiratory cycle. This would be consistent with redox-based molecular mechanisms that have been proposed previously (Rachmilevitch et al., 2004; Bloom, 2015). For example, it is suggested that NR competes poorly against ferredoxin-NADP reductase because it has a lower affinity for ferredoxin, so NO_3^- assimilation is poorer when the CO_2 assimilation is very active. If this is the case, the higher relative consumption of ATP with respect to NADPH shown by photorespiration could translate into weaker competition from NADP reduction. An alternative proposal that the reductant enhances the reduction of NO_3^- to NO_2^- (Bloom, 2015) is similar except that it attributes more of the flux control over NO_3^- assimilation to a different reductase. Thus, our NO_3^- assimilation modes provide a stoichiometric mechanism for this coupling.

The precise balance of CO_2 and O_2 is also preserved when additional reductant is generated in the chloroplast and exported to the cytosol for utilisation by either mitochondrion electron transport or the peroxisomal GSH-ASC cycle. Though extra O_2 is evolved by non-cyclic photophosphorylation, an equivalent amount is absorbed by the mitochondria in respiration, and/or the evolution of O_2 from CAT2 is reduced by the operation of the GSH-ASC cycle.

2.5 Photorespiratory H_2O_2 metabolism and the GSH-ASC Cycle

Although CAT2 is the primary scavenger of photorespiratory H_2O_2 , several studies suggest links between photorespiratory H_2O_2 and peroxidase activity in plants (Wang et al., 1999; Asada, 1999; Mittler, 2002; Sousa et al., 2015) while others have reported photoinactivation of the enzyme catalase in plant cells and cyanobacteria (Tytler et al., 1984; Feierabend and Engel, 1986). We obtained modes with reduced CAT activity and the simultaneous operation of the peroxisomal GSH-ASC pathway for H_2O_2 metabolism. These modes correspond to a higher QD due to the increased redox demand, compared to the catalase route for glutathione reductase of the GSH-ASC pathway (Table 2). The additional reductant for operation of the GSH-ASC cycle is in direct competition with that for NO_3^- reduction, and as the two processes do not otherwise overlap, we do not obtain any photorespiratory EFMs that carry

out both processes together. That is not to say that the two processes cannot occur simultaneously to some degree in the plant, just that they have no direct coupling.

3 Conclusions

The cellular model of C3 plant metabolism yielded 56 EFMs that constitute a comprehensive set of all stoichiometrically feasible routes of photorespiration, subject to the requirement that the process ensures carbon maintenance in the Calvin cycle intermediates so that simultaneous photoassimilation is not progressively compromised. A subset of these corresponds to the canonical C2 pathway with minor variations in the precise quantitative involvement of cyclic and non-cyclic photophosphorylation and mitochondrial redox metabolism. However, we also found additional variants that have the photorespiratory cycle coupled to NO_3^- assimilation, cytosolic ATP generation and the GSH-ASC cycle. They all retain a common core of reactions, which corresponds almost exactly to the set of enzymes that are known from experiment to have a photorespiratory phenotype when mutated. Though all these modes are stoichiometrically feasible and therefore able to make a contribution to photorespiratory metabolism, enzyme kinetic characteristics, environmental conditions and the plant's regulatory mechanisms will all play a role in determining which modes are operational in given circumstances. Nevertheless, this report describes a single computational framework that can simultaneously account for couplings between photorespiration, nitrogen metabolism, mitochondrial respiration and ascorbate metabolism, all of which have considerable experimental support.

Finally, it is interesting to speculate why a structural modelling method such as EFMA is able to elucidate a subtle aspect of plant physiology such as the coupling of photorespiration with NO_3^- assimilation when it uses no information about enzyme kinetics and metabolic regulation. One possibility is that the stoichiometric constraints on autotrophic metabolism, and in particular terrestrial plant metabolism, are particularly strong relative to those on animal or microbial metabolism. That is, the major metabolic inputs are a few inorganic molecules with simple empirical formulae, thus giving a small number of exact stoichiometric ratios between the elements as they are taken in (for example two oxygens with every carbon etc). From these inputs, plant biomass has to be generated that has its own, much less constrained elemental ratio, and in particular a much lower oxygen content. Metabolism has to reconcile these differences; one mechanism is through generating excretory products to carry away the unwanted material, but apart from oxygen, terrestrial plants have limited possibilities to do this beyond some limited storage in the vacuole. As a result, plant metabolism may be much more constrained than that of a heterotrophic bacterium that can excrete a range of products such as acetate or lactate when its carbon catabolism is out of balance with its anabolism and energy requirements. If this is the case, then structural modelling may continue to make further contributions to the understanding of plant metabolism.

4 Methodology

4.1 Software and Analysis

All computation was achieved using the software package ScrumPy - metabolic modelling in Python (Poolman, 2006). This includes modules for constructing and checking metabolic models and computing EFMs. The package, and further information can be obtained from <http://mudshark.brookes.ac.uk/ScrumPy> or by contacting MGP.

The EFMs are computed with arbitrary precision rational arithmetic, so that all the stoichiometric coefficients of reactants and products in the overall equation for the mode, and the relative rates of the participating reactions, are exact arbitrary precision rational numbers, hence avoiding potential rounding errors that would otherwise preclude exact atomic balancing. However, as many of the modes have overall stoichiometric equations with large coefficients that differ from mode to mode, comparisons of different modes have been made by scaling to a unit of Rubisco oxygenase flux resulting in decimal numbers with rounding.

4.2 Model Construction

We developed a model centered on the reactions of the C2 cycle, constructed in a modular fashion, consisting of chloroplast, mitochondrial and peroxisomal models along with a minimal model of the cytosolic compartment to act primarily as the medium for metabolites to interchange between the organelles (see Methods S1).

Once the organelle models were working separately, they were combined as a cellular model, the EFMs of which were calculated with no carbon-containing metabolites defined as externals, so there could be no net photoassimilation. The overall reactions of the modes could be expressed in terms of the extracellular resources such as photons, CO₂, O₂, H₂O, NH₄⁺ and NO₃⁻, as well as the dummy metabolites monitoring the fluxes of the rubisco carboxylase and oxygenase, and the cytosolic ATPase.

Based on their occurrence in the set of EFMs, the reactions of the cellular model were classified using the Python analysis code within ScrumPy as:

1. Reactions that occur in all of the EFMs and hence are essential for photorespiration, since an EFM can only function if all of its reactions are active, and therefore inactivation of any of these reactions leaves no photorespiratory modes.
2. Reactions that carry flux in some but not all of the photorespiratory modes so are potentially involved, but may not be essential as there are other photorespiratory modes that could function if the reactions were inhibited or knocked out, and
3. 'Dead reactions' (Fell et al., 2010) that do not carry flux in any functioning photorespiratory mode, that is, they have been included in the organelle models as components of their characteristic metabolism, but they have turned out not to participate in photorespiration.

Acknowledgements

This work was supported by grants to: DAF from the UK's Biotechnology and Biological Sciences Research Council (grant references BB/E00203X/1 and BB/G530317/1); SK from India's Department of Biotechnology (Crest Fellowship BT/IN/CREST Awards/38/SK/2010-11) and Centre of Excellence in Systems Biology and Biomedical Engineering, (TEQIP, Phase-II), University of Calcutta and BH from the Department of Science and Technology INSPIRE Research Fellowship (DST/INSPIRE Fellowship/2013/653) Oxford Brookes University and the University of Calcutta also provided research support to DAF, MGP and SK.

Conflict of Interest

The authors declare that no conflict of interest exists.

Supporting Information

Figures S1 and S2: Illustrating the classification of the modes into groups based on stoichiometry and reaction involvement.

Figures S3, S4 and S5: Additional pathway diagrams of the EFMs using the alternative oxidase (AOX) component of the mitochondrial electron transport chain; counterparts to the main text figures with the AOX used in place of the cytochrome oxidase (COX).

Table S1: Reaction, transporter and metabolite counts for the organelle and cellular models.

Table S2: Minimal chloroplast energy requirements for photorespiration.

Data S1: An archive file, Model.zip, containing the organelle and cellular photorespiratory models in ScrumPy format, text and SBML format with some explanatory text in a README file and analysis script in python used to perform further analysis of the EFMs.

Data S2: Spreadsheets detailing the EFMs in terms of their reaction fluxes and the stoichiometries of their overall reactions.

Methods S1: Additional information for the methodology used for model construction, generation and analysis of organelle EFMs.

Appendix S1: Extended Results and Discussions.

References

Aliyev, J. A. (2012) Photosynthesis, photorespiration and productivity of wheat and soybean genotypes. *Physiologia plantarum*, **145**, 369–383.

Asada, K. (1999) The water-water cycle in chloroplasts: scavenging of active oxygens and dissipation of excess photons. *Annu. Rev. Plant biol.*, **50**, 601–639.

- Bauwe, H., Hagemann, M., Kern, R. and Timm, S.** (2012) Photorespiration has a dual origin and manifold links to central metabolism. *Curr. Opin. Plant Biol.*, **15**, 269–75.
- Bloom, A. J.** (2015) Photorespiration and nitrate assimilation: a major intersection between plant carbon and nitrogen. *Photosyn. Res.*, **123**, 117–28.
- Boldt, R., Edner, C., Kolukisaoglu, U., Hagemann, M., Weckwerth, W., Wienkoop, S., Morgenthal, K. and Bauwe, H.** (2005) D–Glycerate 3–kinase, the last unknown enzyme in the photorespiratory cycle in Arabidopsis, belongs to a novel kinase family. *The Plant Cell*, **17**, 2413–2420.
- Busch, F. A., Sage, R. F. and Farquhar, G. D.** (2017) Plants increase CO₂ uptake by assimilating nitrogen via the photorespiratory pathway. *Nature Plants*, **10.1038/s41477-017-0065-x**.
- Busch, F. A., Sage, T. L., Cousins, A. B. and Sage, R. F.** (2013) C₃ plants enhance rates of photosynthesis by reassimilating photorespired and respired CO₂. *Plant Cell Environ.*, **36**, 200–212.
- Cheung, C. Y. M., Williams, T. C. R., Poolman, M. G., Fell, D. A., Ratcliffe, R. G. and Sweetlove, L. J.** (2013) A method for accounting for maintenance costs in flux balance analysis improves the prediction of plant cell metabolic phenotypes under stress conditions. *Plant J*, **75**, 1050–61.
- Delfine, S., Di Marco, G. and Loreto, F.** (1999) Estimation of photorespiratory carbon dioxide recycling during photosynthesis. *Functional Plant Biology*, **26**, 733–736.
- Duttilleul, C., Driscoll, S., Cornic, G., Paepe, R. D., Foyer, C. H. and Noctor, G.** (2003) Functional mitochondrial complex I is required by tobacco leaves for optimal photosynthetic performance in photorespiratory conditions and during transients. *Plant Physiol.*, **131**, 264–75.
- Engel, N., van den Daele, K., Kolukisaoglu, U., Morgenthal, K., Weckwerth, W., Pärnik, T., Keerberg, O. and Bauwe, H.** (2007) Deletion of glycine decarboxylase in Arabidopsis is lethal under nonphotorespiratory conditions. *Plant Physiol.*, **144**, 1328–35.
- Feierabend, J. and Engel, S.** (1986) Photoinactivation of catalase *in vitro* and in leaves. *Arch. Biochem. Biophys.*, **251**, 567–576.
- Fell, D. and Small, J. R.** (1986) Fat synthesis in adipose tissue: an examination of stoichiometric constraints. *Biochem. J.*, **238**, 781–786.
- Fell, D. A., Poolman, M. G. and Gevorgyan, A.** (2010) Building and analysing genome-scale metabolic models. *Biochem. Soc. Trans.*, **38**, 1197–1201.
- Florian, A., Araújo, W. L. and Fernie, A. R.** (2013) New insights into photorespiration obtained from metabolomics. *Plant Biol.*, **15**, 656–66.
- Foyer, C. H., Bloom, A. J., Queval, G. and Noctor, G.** (2009) Photorespiratory metabolism: genes, mutants, energetics, and redox signaling. *Annu. Rev. Plant Biol.*, **60**, 455–484.
- Givan, C. V., and Kleczkowski, L. A.** (1992) The enzymic reduction of glyoxylate and hydroxypyruvate in leaves of higher plants. *Plant Physiol.*, **100**, 552–556.

Hodges, M., Deller, Y., Keech, O., Betti, M., Raghavendra, A. S., Sage, R., Zhu, X.-G., Allen, D. K. and Weber, A. P. M. (2016) Perspectives for a better understanding of the metabolic integration of photorespiration within a complex plant primary metabolism network. *J. Exp. Bot.*, **67**, 3015–3026.

Hurry, Vaughan and Igamberdiev, Abir U and Keerberg, Olav and Pärnik, Tiit and Atkin, Owen K and Zaragoza-Castells, Joana and Gardeström, P. (2005) Respiration in photosynthetic cells: gas exchange components, interactions with photorespiration and the operation of mitochondria in the light. In *Plant respiration*, pp. 43–61. Springer.

Igarashi, D., Miwa, T., Seki, M., Kobayashi, M., Kato, T., Tabata, S., Shinozaki, K. and Ohsumi, C. (2003) Identification of photorespiratory glutamate: glyoxylate aminotransferase (GGAT) gene in Arabidopsis. *Plant J.*, **33**, 975–987.

Jamai, A., Salomé, P. A., Schilling, S. H., Weber, A. P. M. and McClung, C. R. (2009) Arabidopsis photorespiratory serine hydroxymethyltransferase activity requires the mitochondrial accumulation of ferredoxin-dependent glutamate synthase. *Plant Cell*, **21**, 595–606.

Liepmann, A. H. and Olsen, L. J. (2001) Peroxisomal alanine: glyoxylate aminotransferase (AGT1) is a photorespiratory enzyme with multiple substrates in Arabidopsis thaliana. *Plant J.*, **25**, 487–98.

Lindén, P., Keech, O., Stenlund, H., Gardestrom, P. and Moritz, T. (2016) Reduced mitochondrial malate dehydrogenase activity has a strong effect on photorespiratory metabolism as revealed by C-13 labelling. *J. Exp. Bot.*, **67**, 3123–3135.

Lu, Y., Li, Y., Yang, Q., Zhang, Z., Chen, Y., Zhang, S. and Peng, X.-X. (2014) Suppression of glycolate oxidase causes glyoxylate accumulation that inhibits photosynthesis through deactivating Rubisco in rice. *Physiol. Plantarum*, **150**, 463–476.

Mittler, R. (2002) Oxidative stress, antioxidants and stress tolerance. *Trends Plant Sci.*, **7**, 405–410.

Noctor, G. and Foyer, C. H. (1998) A re-evaluation of the ATP: NADPH budget during C3 photosynthesis: a contribution from nitrate assimilation and its associated respiratory activity? *J. Exp. Bot.*, **49**, 1895–1908.

Oliver, D. J. (2000) Photorespiration and the C2 Cycle. In **Raghavendra, A. S.**, ed., *Photosynthesis: a Comprehensive Treatise*, pp. 173–182. Cambridge: Cambridge University Press.

Pick, T. R., Bräutigam, A., Schulz, M. A., Obata, T., Fernie, A. R. and Weber, A. P. M. (2013) PLGG1, a plastidic glycolate glycerate transporter, is required for photorespiration and defines a unique class of metabolite transporters. *Proc. Natl. Acad. Sci. U.S.A.*, **110**, 3185–90.

Poolman, M. G. (2006) ScrumPy - metabolic modelling with Python. *IEE Proc. Syst. Biol.*, **153**, 375–378.

Poolman, M. G., Kundu, S., Shaw, R. and Fell, D. A. (2013) Responses to light intensity in a genome-scale model of rice metabolism. *Plant Physiol.*, **162**, 1060–72.

Poolman, M. G., Kundu, S., Shaw, R. and Fell, D. A. (2014) Metabolic trade-offs between biomass synthesis and photosynthate export at different light intensities in a genome-scale metabolic model of rice. *Front. Plant Sci.*, **5**, 656.

Poolman, M. G., Miguet, L., Sweetlove, L. J. and Fell, D. A. (2009) A genome-scale metabolic model of Arabidopsis and some of its properties. *Plant Physiol*, **151**, 1570– 81.

Poolman, M. G., Sebu, C., Pidcock, M. K. and Fell, D. A. (2007) Modular decomposition of metabolic systems via null-space analysis. *Journal of theoretical biology*, **249**, 691–705.

Queval, G., Issakidis-Bourguet, E., Hoerberichts, F. A., Vandorpe, M., Gakière, B., Vanacker, H., Miginiac-Maslow, M., Van Breusegem, F. and Noctor, G. (2007) Conditional oxidative stress responses in the Arabidopsis photorespiratory mutant cat2 demonstrate that redox state is a key modulator of daylength-dependent gene expression, and define photoperiod as a crucial factor in the regulation of H₂O₂induced cell death. *Plant J.*, **52**, 640–657.

Rachmilevitch, S., Cousins, A. B. and Bloom, A. J. (2004) Nitrate assimilation in plant shoots depends on photorespiration. *Proc. Natl. Acad. Sci. U.S.A.*, **101**, 11506–10.

Renné, P., Dressen, U., Hebbeker, U., Hille, D., Flügge, U.-I., Westhoff, P. and Weber, A. P. M. (2003) The Arabidopsis mutant dct is deficient in the plastidic glutamate/malate translocator DiT2. *Plant J.*, **35**, 316–31.

Riazunnisa, K., Padmavathi, L., Bauwe, H. and Raghavendra, A. S. (2006) Markedly low requirement of added CO₂ for photosynthesis by mesophyll protoplasts of pea (*Pisum sativum*): possible roles of photorespiratory CO₂ and carbonic anhydrase. *Physiologia plantarum*, **128**, 763–772.

Schilling, C., Schuster, S., Palsson, B. and Heinrich, R. (1999) Metabolic pathway analysis: basic concepts and scientific applications in the post-genomic era. *Biotechnol. Prog.*, **15**, 296–303.

Schneidereit, J., Häusler, R. E., Fiene, G., Kaiser, W. M. and Weber, A. P. M. (2006) Antisense repression reveals a crucial role of the plastidic 2-oxoglutarate/malate translocator DiT1 at the interface between carbon and nitrogen metabolism. *Plant J.*, **45**, 206–24.

Schuster, S., Dandekar, T. and Fell, D. (1999) Detection of elementary flux modes in biochemical networks: a promising tool for pathway analysis and metabolic engineering. *Trends. Biotech.*, **17**, 53–60.

Schuster, S., Fell, D. and Dandekar, T. (2000) A general definition of metabolic pathways useful for systematic organization and analysis of complex metabolic networks. *Nature Biotech.*, **18**, 326–332.

Schuster, S. and Fell, D. A. (2007) Modelling and simulating metabolic networks. In **Lengauer, T.**, ed., *Bioinformatics: From Genomes to Therapies*, volume 2, chapter 20, pp. 755–806. Weinheim: Wiley–VCH.

Schwarte, S. and Bauwe, H. (2007) Identification of the photorespiratory 2phosphoglycolate phosphatase, PGLP1, in Arabidopsis. *Plant Physiol.*, **144**, 1580– 1586.

- Searles, P. S. and Bloom, A. J.** (2003) Nitrate photo-assimilation in tomato leaves under short-term exposure to elevated carbon dioxide and low oxygen. *Plant Cell Environ.*, **26**, 1247–1255.
- Skillman, J. B.** (2008) Quantum yield variation across the three pathways of photosynthesis: not yet out of the dark. *J. Exp. Bot.*, **59**, 1647–61.
- Sousa, R. H. V., Carvalho, F. E. L., Ribeiro, C. W., Passaia, G., Cunha, J. R., Lima-Melo, Y., Margis-Pinheiro, M. and Silveira, J. A. G.** (2015) Peroxisomal APX knockdown triggers antioxidant mechanisms favourable for coping with high photorespiratory H₂O₂ induced by CAT deficiency in rice. *Plant Cell Environ.*, **38**, 499–513.
- Taniguchi, M., Taniguchi, Y., Kawasaki, M., Takeda, S., Kato, T., Sato, S., Tabata, S., Miyake, H. and Sugiyama, T.** (2002) Identifying and characterizing plastidic 2-oxoglutarate/malate and dicarboxylate transporters in *Arabidopsis thaliana*. *Plant Cell Physiol.*, **43**, 706–17.
- Timm, S., Nunes-Nesi, A., Pärnik, T., Morgenthal, K., Wienkoop, S., Keerberg, O., Weckwerth, W., Kleczkowski, L. A., Fernie, A. R. and Bauwe, H.** (2008) A cytosolic pathway for the conversion of hydroxypyruvate to glycerate during photorespiration in *Arabidopsis*. *Plant Cell*, **20**, 2848–59.
- Tytler, E., Wong, T. and Codd, G.** (1984) Photoinactivation in vivo of superoxide dismutase and catalase in the cyanobacterium *Microcystis aeruginosa*. *FEMS Microbiol. Lett.*, **23**, 239–242.
- Ushijima, T., Hanada, K., Gotoh, E., Yamori, W., Kodama, Y., Tanaka, H., Kusano, M., Fukushima, A., Tokizawa, M., Yamamoto, Y.Y. and Tada, Y.** (2017) Light controls protein localization through phytochrome-mediated alternative promoter selection. *Cell*, **171**, 1316–1325.
- Varma, A. and Palsson, B. O.** (1993) Metabolic capabilities of *Escherichia coli*: I. synthesis of biosynthetic precursors and cofactors. *J. Theor. Biol.*, **165**, 477–502.
- Voll, L. M., Jamai, A., Renné, P., Voll, H., McClung, C. R. and Weber, A. P. M.** (2006) The photorespiratory *Arabidopsis* *shm1* mutant is deficient in SHM1. *Plant Physiol.*, **140**, 59–66.
- Voss, I., Sunil, B., Scheibe, R. and Raghavendra, A.** (2013) Emerging concept for the role of photorespiration as an important part of abiotic stress response. *Plant Biol.*, **15**, 713–722.
- Wallsgrave, R. M., Turner, J. C., Hall, N. P., Kendall, A. C. and Bright, S. W.** (1987) Barley mutants lacking chloroplast glutamine synthetase-biochemical and genetic analysis. *Plant Physiol.*, **83**, 155–8.
- Wang, J., Zhang, H. and Allen, R. D.** (1999) Overexpression of an *Arabidopsis* peroxisomal ascorbate peroxidase gene in tobacco increases protection against oxidative stress. *Plant Cell Physiol.*, **40**, 725–732.
- Wingler, A., Lea, P. J., Quick, W. P. and Leegood, R. C.** (2000) Photorespiration: metabolic pathways and their role in stress protection. *Philos. T. Roy. Soc. B*, **355**, 1517–1529.

- Wu, J., Zhang, Z., Zhang, Q., Han, X., Gu, X. and Lu, T.** (2015) The molecular cloning and clarification of a photorespiratory mutant, *oscdm1*, using enhancer trapping. *Front. Genet.*, **6**.
- Xin, C.-P., Tholen, D., Devloo, V. and Zhu, X.-G.** (2015) The Benefits of Photorespiratory Bypasses: How Can They Work? *Plant Physiol.*, **167**, 574–585.
- Xu, H., Zhang, J., Zeng, J., Jiang, L., Liu, E., Peng, C., He, Z. and Peng, X.** (2009) Inducible antisense suppression of glycolate oxidase reveals its strong regulation over photosynthesis in rice. *J. Exp. Bot.*, **60**, 1799–1809.
- Ye, N., Yang, G., Chen, Y., Zhang, C., Zhang, J. and Peng, X.** (2014) Two hydroxypyruvate reductases encoded by OsHPR1 and OsHPR2 are involved in photorespiratory metabolism in rice. *J. Integr. Plant Biol.*, **56**, 170–180.
- Zabaleta, E., Martin, M. V. and Braun, H.-P.** (2012) A basal carbon concentrating mechanism in plants? *Plant Science*, **187**, 97–104.
- Zelitch, I.** (1973) Plant productivity and control of photorespiration. *Proc. Natl. Acad. Sci. U.S.A.*, **70**, 579–584.
- Zelitch, I., Schultes, N. P., Peterson, R. B., Brown, P. and Brutnell, T. P.** (2009) High glycolate oxidase activity is required for survival of maize in normal air. *Plant Physiol.*, **149**, 195–204.
- Zhang, Z., Mao, X., Ou, J., Ye, N., Zhang, J. and Peng, X.** (2015) Distinct photorespiratory reactions are preferentially catalyzed by glutamate:glyoxylate and serine:glyoxylate aminotransferases in rice. *J. Photoch. Photobio. B*, **142**, 110–117.

List of Figure Legends

Figure 1: The classic photorespiratory C2 cycle. The recovery of carbon from 2-phosphoglycolate as conventionally viewed. The numeric values next to the reactions show the flux values relative to unit flux in Rubisco oxygenase. Note that the net flux towards RuBP is only 0.9 units, so the pathway as written does not fully replace it, resulting in a gradual depletion of C3/Calvin cycle intermediates and it cannot represent steady state metabolism. Reactions: Chloroplast: r1-r3: the chloroplast-specific reactions of the C2 cycle namely, Rubisco oxygenase, 2-phosphoglycolate phosphatase (PGP1) and glycerate 3-kinase (GLYK), r4-r15: the C3 cycle, r16: glycolate-glycerate translocator (PLGG1). Peroxisome: r17-r21: C2 cycle; r17: glycolate oxidase (GO), r18: catalase (CAT2), r19: glutamate-glyoxylate aminotransferase (GGAT1), r20: serine-glyoxylate aminotransferase (SGAT), r21: hydroxypyruvate reductase (HPR1); r22-r24: metabolite exchange reactions. Mitochondrion: r25: combined reaction for glycine decarboxylase (GDC) and serine hydroxymethyltransferase (SHMT1), r26 and r27: metabolite exchange reactions.

Figure 2: The metabolic model for photorespiration. The metabolic network shown is the aggregate of the three organelle models (chloroplast, mitochondrion and peroxisome) with the common cytosolic compartment. Reactions: r1-r27: as in Fig.1. Chloroplast: r28: Rubisco carboxylase, r29-r30: the cyclic and non-cyclic photophosphorylation reactions, r31: malate

dehydrogenase (MDH), r32: nitrite reductase, r33: ferredoxin (Fd)-NADP reductase, r34-r35: GS2 and Fd-GOGAT, r36: DiT2.1, r37: DiT1, r38: AtpOMT1, r39-r43: metabolite exchange reactions. Cytosol: r44: nitrate reductase (NR), r45: MDH, r46: HPR2, r47-r51: cytosolic exchange reactions for extracellular resource metabolites, r52: ATPase reaction. Mitochondrion: r53-r60: reactions of the TCA cycle, (r55 represents combined reaction catalysed by aconitase), r61: MDH, r62: complex I, r63-r64: cytochrome oxidase (COX), r65: alternative oxidase (AOX), r66: ATP synthase, r67-r75: metabolite exchange reactions. Peroxisome: r76: alanine-glyoxylate aminotransferase (AGAT), r77: alanine aminotransferase, r78: MDH, r79-r81: GSH-ASC cycle, r82-r89: metabolite exchange reactions.

Figure 3: Energy-dissipating modes and ATP producing modes. In this and all other flux maps, the following conventions are used: dark lines represent the set of reactions constituting a steady-state metabolic mode with the numeric values giving their relative fluxes and grey lines represent reactions of the model which carry no flux in the modes illustrated. The flux values in black are those common to the modes shown. Flux values shown in a box of a given colour are specific to a particular mode. Two EFMs have been shown here, an energy-dissipating mode (blue) with no net metabolic effect and a similar mode producing photorespiratory (PR) ATP (red). The modes shown here and other figures of the main text use the cytochrome oxidase (COX (blue)) component of mitochondrial electron transport chain; their alternative oxidase (AOX (yellow)) counterparts can be found in the supporting figures (Figs. S3, S4 and S5). The equivalent modes using reactions r76 and r77 are not illustrated. Equivalent modes for the illustrated EFMs that use HPR2 and associated reactions instead of HPR1 and associated reactions (flux values in hexagon) are shown with flux values in ellipses.

Figure 4: Energy-dissipating modes and O₂ producing modes. In these modes, non-cyclic photophosphorylation is active while cyclic photophosphorylation remains inactive and mitMDH operates in reverse (mitMDH -ve) to meet the ATP:NAPDH demand of the C2 cycle. Colour and line conventions are as in Fig. 3 except that fluxes in blue boxes are common to both modes but highlight the use of COX instead of the AOX component of mitochondrial electron transport chain. Flux values specific to nitrate assimilation are in green boxes (including net O₂ evolution) and those specific to the energy-dissipating modes which involve the GSH-ASC cycle, are in pink. Equivalent modes using HPR2 and associated reactions are shown with flux values in ellipses.

Figure 5: Photorespiratory EFMs generating cytosolic ATP. In these modes, non-cyclic photophosphorylation alone meets the chloroplast energy demand, i.e the cyclic light reaction is inactive. This generates excess reductant which can be reoxidised in the mitochondrion giving the highest yield of ATP (red), with mitMDH operating in the forward direction. Otherwise, part of the excess reductant can be used for nitrate assimilation (O₂ producing modes in green) and part for ATP (blue), or else part can be consumed in the GSH-ASC cycle (pink), again with net ATP production (blue). In these latter cases, there is no flux through mitMDH. Colours and line conventions are as in Fig. 3, except that flux values common to both the nitrate assimilation and GSH-ASC modes but not to the solely ATP-generating mode are shown in blue.

Tables

Table 1: Mutant enzymes and their photorespiratory phenotype. Summary of experimental studies determining the presence (Y) or absence (N) of a photorespiratory phenotype are compared with reaction essentiality for photorespiration according to the model. Expanded from Foyer et al. (2009) and Hodges et al. (2016). The case of hydroxypyruvate reductase is discussed in the main text.

Enzyme	Arabidopsis	Rice	Other	Essential in model
Carbon metabolism				
2-Phosphoglycolate phosphatase (PGP1)	Y; Schwarte and Bauwe (2007)			Y
Glycolate oxidase (GO)		Y; Xu et al. (2009); Lu et al. (2014)	Y, maize; Zelitch et al. (2009)	Y
Glutamate-glyoxylate aminotransferase (GGAT1)	Y; Igarashi et al. (2003)	Y; Zhang et al. (2015)		N
Serine-glyoxylate aminotransferase (SGAT)	Y; Liepman and Olsen (2001)			Y
Serine hydroxymethyltransferase (SHMT1)	Y; Voll et al. (2006)	Y; Wu et al. (2015)		Y
Glycine decarboxylase (GDC)	Y; Engel et al. (2007)			Y
Hydroxypyruvate reductase (HPR1)	N; Timm et al. (2008)	N; Ye et al. (2014)		N
HPR1 + HPR2	Y; Timm et al. (2008)	Y; Ye et al. (2014)		Y
Glycerate kinase (GLYK)	Y; Boldt et al. (2005)			Y
Mit-MDH	Y; Lindén et al. (2016)			N
Hydrogen peroxide metabolism				

Catalase (CAT2)	Y; Queval et al. (2007)			Y
Nitrogen Cycle				
Glutamate synthase (Fd-GOGAT)	Y; Jamaï et al. (2009)			Y
Glutamine synthetase (GS2)			Y, barley; Wallsgrave et al. (1987)	Y
Transporters				
Plastidic glutamate-malate translocator (DiT2.1)	Y; Renné et al. (2003); Y; Taniguchi et al. (2002)			Y
Plastidic oxoglutarate-malate translocator (DiT1)	Y; Taniguchi et al. (2002)		Y; tobacco; Schneidereit et al. (2006)	Y
Chloroplastic oxaloacetate transporter (AtpOMT1)	N; Taniguchi et al. (2002)			Y
Chloroplastic glycolate-glycerate transporter (PLGG1)	Y; Pick et al. (2013)			Y

Table 2: Stoichiometries of representative photorespiratory elementary flux modes. Flux units and stoichiometric yields are normalised to one mole of CO₂ fixed, i.e. unit flux through the Rubisco carboxylase reaction. This corresponds to double the flux in the Rubisco oxygenase reaction, so fluxes per mole of O₂, as shown in the figures, are half the values in this table. One unit of flux in the non-cyclic light reaction corresponds to 14 photons absorbed, and in the cyclic light reaction to 7 photons absorbed. EFM types: A = use of AOX; C = use of COX; E = energy-dissipating; G = uses GSH-ASC cycle; N = NO₃⁻ assimilation; P = ATP-producing.

Quantum Demand	Quantum Yield	EFM type	Flux map	Non-cyclic light reaction	Cyclic light reaction	ATP formed	NADPH formed	ATP:NA DPH	NO ₃ ⁻ flux	Net O ₂ flux	ATP cytosol
29.4	0.034	C, E	Fig. 3 (blue)	1.742	0.718	10.0	6.097	1.640	0.0	0.0	0.0
29.6	0.034	A, E	Fig. S3 (yellow)	1.786	0.654	10.0	6.251	1.6	0.0	0.0	0.0
30.3	0.033	C, P	Fig. 3 (red)	2.0	0.334	10.0	7.00	1.429	0.0	0.0	4.2
30.3	0.033	A, P	Fig. S3 (red)	2.0	0.334	10.0	7.00	1.429	0.0	0.0	1.53
31.1	0.032	A, C, E, G	Figs. 4, S4 (pink)	2.222	0.0	10.0	7.78	1.285	0.0	0.0	0.0
31.1	0.032	C, G, P	Fig. 5 (pink/blue)	2.222	0.0	10.0	7.78	1.285	0.0	0.0	2.25
31.1	0.032	A, G, P	Fig. S5 (pink/yellow)	2.222	0.0	10.0	7.78	1.285	0.0	0.0	0.75
31.1	0.032	C, N	Fig. 4 (green/blue)	2.222	0.0	10.0	7.78	1.285	0.418	0.838	0.0

